

Effect of Processing Medium and Condition on Absorption Enhancement of Femtosecond Laser Treated a-Si:H Thin Film

Hongliang Wang, Panjawat Kongsuwan, Gen Satoh, Y. Lawrence Yao
Department of Mechanical Engineering
Columbia University
New York, NY, USA

ABSTRACT

Hydrogenated amorphous silicon (a-Si:H) thin films have been considered for use in solar cell applications because of their significantly reduced cost compared to crystalline bulk silicon, however, their overall efficiency and stability are less than that of their bulk crystalline counterparts. Limited work has been performed on simultaneously solving the efficiency and stability issues of a-Si:H. Surface texturing and crystallization on a-Si:H thin film can be achieved through one-step femtosecond laser processing, which can potentially alleviate the disadvantages of a-Si:H in solar cell applications. In this study, submicrometer conical and pillar-shaped spikes are fabricated by irradiating a-Si:H thin films deposited on glass substrates with hundreds of 800nm-wavelength, 130fs-duration laser pulses in air and water environments, respectively. Enhanced light absorption is observed due to light trapping based on surface geometry changes, while the formation of a mixture of hydrogenated nanocrystalline silicon (nc-Si:H) and a-Si:H after crystallization suggests that the overall material stability can potentially be increased. The relationship between crystallinity, fluence and scanning speed is also discussed. Furthermore, a comparison of absorptance spectra for various surface morphologies is performed. Finally, absorptance measurements across the solar spectrum show that the combination of surface texture and crystallinity induced by femtosecond laser processing is very promising for a-Si:H thin film solar cell applications.

INTRODUCTION

Many industrial solar cells in use today use bulk materials as absorbers with crystalline silicon being the most prevalent. Crystalline silicon, however, suffers from the disadvantage of high material cost since relatively large thicknesses are required primarily due to its low absorption coefficient. Recently, thin film absorbers are becoming more attractive based on their potential for low-cost modules, tandem junctions, and large-scale manufacturability [1-3]. a-Si:H is the most popular material for use in thin film form due to its low energy economy (cost/watt). The main issue with a-Si:H is the high order of dangling bonds which act as recombination centers that severely reduce the carrier lifetime which results in the efficiency being below 10%. Additionally, this initial efficiency will decrease by 50% or more when exposed to sunlight over a period of several months which is known as the Staebler-Wronski effect or SWE [4-5].

Due to their low efficiency and instability, thin-film a-Si:H solar cells require a highly efficient light-trapping design to absorb a significant fraction of the incident sunlight and material property changes to increase stability against the SWE. Antireflection (AR) coatings and front-side texturing through the use of alkaline-based solutions, such as KOH and NaOH etching have been used on crystalline silicon solar cells, and pulsed laser irradiation

has been used to enhance light trapping on both amorphous and crystalline materials [6-9]. AR coating, however, requires additional material and anisotropic wet chemical etching is not applicable for amorphous materials or thin films. While surface texturing by laser treatment is able to improve the efficiency of solar cells, the SWE still remains. The most important material properties that play a role in the SWE are the high disorder in the Si network and high concentration of impurities, which cause some atoms to have dangling bonds that act as defects. Although these dangling bonds can be passivated by hydrogen, light exposure generates electron hole pairs that will combine and the released energy can break the Si-H bond and promote H to a transport state. The diffusing H-atom successively breaks Si-Si bonds creating Si-H bonds and a neighboring dangling bond. This increasing defect density caused by the so-called SWE works to further reduce the cell efficiency [4, 10]. In order to reduce the SWE, hybrid a-Si/nc-Si tandem modules have been developed and are able to achieve both higher efficiency and stability compared with single junction a-Si:H due to the use of a thinner a-Si layer and the wider spectral absorption of nc-Si [11]. To eliminate the need for two separate deposition steps which are required to form these tandem cells, laser-induced crystallization of a-Si:H has been proposed to produce a mixture of nc-Si:H and a-Si:H and simultaneously form a light trapping texture on the surface

of the material [8, 12]. Therefore, laser-based treatment of a-Si:H may solve its efficiency and stability issues in a one-step process, which is a promising methodology for thin-film solar cell fabrication.

Surface texturing can be achieved by both femtosecond and long-pulse lasers, however, femtosecond lasers are better suited for precise micromachining due to their extremely high peak power and ultrashort pulse duration, which leads to greatly reduced thermal energy diffusion and heat-affected-zone and allows for precise control over the texturing process [13-14]. Therefore, for texturing films of limited thickness, femtosecond laser processing is more desirable. Extensive work on surface texturing of crystalline bulk silicon had been reported by Mazur, et al. [15-16]. Micron-size conical spikes have been generated on crystalline silicon a few hundred-micrometers thick when irradiated with a femtosecond laser in different background gases, such as SF₆, N₂, and air, and a significant enhancement in light absorptance is achieved after texturing. The formation of submicron spikes and ripples with periodicity in the nano-scale on crystalline silicon has also been investigated after femtosecond laser irradiation in water, and has been shown to produce much denser spikes than when processed in a gas environment [17-18]. However, limited work is presented for a-Si:H thin films. Nayak, et al. [12] showed the observation of crystallization and simultaneous formation of irregular nano-sizes spikes on roughly 2µm-thick a-Si:H thin films through femtosecond laser processing in air; Wang, et al. [8] showed crystallization and the formation of densely packed pillar-shaped spikes on 1.6µm-thick a-Si:H thin films through femtosecond laser irradiation in water; both experiments showed that the textured spikes resulted in similar absorption enhancement to that observed for laser processed crystalline bulk silicon. The light absorption for different surface geometries on a-Si:H surfaces, however, has not been characterized after laser irradiation in different processing environments, such as background gases and water.

In this paper, a-Si:H thin films deposited on glass substrates are irradiated with different numbers of femtosecond laser pulses at various fluences in air and water, and the formation of conical and pillar-shaped spiked surface structures is observed. The feature characteristics are studied through scanning electron microscopy (SEM) and atomic force microscopy (AFM) for different processing environments. Furthermore, the dependence of light absorptance on surface structure is studied by spectrophotometry while the effect of laser processing on crystallinity is investigated by x-ray diffractometry (XRD). The combined effects of light trapping surface structures and crystallization on a-Si:H suggests a one-step process for enhancing the efficiency and stability of thin film solar cells.

BACKGROUND

Surface texturing mechanism

Most micromachining work under the ablation regime is performed by removing material within the irradiated area and generating a crater. However, under some certain conditions, the laser can induce periodic surface structures with periodicity much smaller than the spot size. Extensive work has been performed on femtosecond laser induced surface texturing of crystalline bulk silicon, and Nayak, et al. [12] and Wang, et al. [8] believed that the formation mechanism was also suitable for surface texturing of a-Si:H in air and water. However, comparing thin film and bulk samples, the processing conditions are more critical for thin films since the entire film must not be removed during the process. Additionally, based on the difference in thermal properties between amorphous and crystalline materials, the periodicity of the final texture on a-Si:H should be different, especially for underwater treatment. The two stage texture formation mechanism for crystalline bulk silicon has been described by Mazur, et al. [17, 19] who showed spike formation on crystalline silicon surfaces by femtosecond laser irradiation in both gas and water environments. During the first stage of processing in a gas environment, straight, wavelength-dependent ripple structures are first formed on the silicon surface which is called light-induced periodic surface structure (LIPSS). With semiconductors, the ripples are mainly orientated perpendicular to the electric field vector of the incident laser beam and the period can be predicted by [20]:

$$\Lambda \approx \frac{\lambda}{1 \pm \sin \theta_i} \quad \text{for s-polarized light} \quad (1)$$

$$\Lambda \approx \frac{\lambda}{\cos \theta_i} \quad \text{for p-polarized light} \quad (2)$$

where, Λ is the spacing between adjacent ripples, λ is laser wavelength, and θ_i is the incident angle. After the formation of LIPSS, micron-scale ridges are generated on the top of and perpendicular to the ripples. The coarsened layer breaks up into micron-size beads which is suggested to be caused by surface tension effects [19]. For a water environment, in the first stage, most of the light is absorbed by a silicon layer tens of nanometers thick near the silicon-water interface which creates a plasma. Due to the high temperature of the plasma, micro-size bubbles are generated by the decomposition of water. Diffraction of the laser beam by these bubbles produces ripple-like structures on the silicon surface due to the existence of high and low intensity fringes. The separation between adjacent rings is found to be close to the wavelength of the laser. Roughness on the silicon surface causes the laser pulse energy to be non-uniformly absorbed across the surface, which results in a random arrangement of bubbles. The superposition of ripple structures generated by multiple laser pulses causes

bead-like structures to be randomly distributed on the surface of the material.

The second stage of surface structure formation is similar for processing in both gas and water environments. The beads that formed in the first stage act to concentrate subsequent laser light into the valleys between them through reflection off the sides of the beads. This causes the ablation rate to be higher inside the valleys than on the bead tips, which leads to sharpening of the beads into spikes after hundreds of laser pulse assisted texturing steps. It is noted that, in water, the spikes are generated with submicron heights and wavelength-dependent spacing and are much shorter and denser than those formed in gas environments.

Factors affecting light absorption

The light absorption capabilities of a material depend on its optical properties (refractive index, absorption coefficient), film thickness, and surface roughness. This paper mainly focuses on a-Si:H, and thus the optical properties are considered to be consistent between samples. As known, the thicker the film, the higher the light absorption. However, a thick a-Si:H layer increases the number of recombination centers. As a result, the stability performance deteriorates and the cost increases. Anti-reflection coating is also a way to improve absorption, but additional costs for the material and deposition process are also introduced. Therefore, changing the material surface geometry is the most economical and efficient way for enhancing the light absorbance.

Yagi, et al. [21] showed a significant reduction in the reflectance of crystalline silicon with a pyramidal textured surface by anisotropic etching, and also found that the reflectance of silicon deposited on V-shaped glass substrates increases with increasing angle of the V-shape. Halbawx, et al. [22] investigated the dependence of absorption on different shape surface structures and showed conical spikes had the best absorption performance, followed by pillars and pyramids. Hua, et al. [23] investigated the absorption caused by different surface geometries and found that surface structures with higher density, smaller top angle, and a spike shape that can introduce a greater number of reflections within the periodic structures will absorb a larger fraction of the incoming light.

From the discussion above, it is clear that the spikes formed in air and water have their own advantages and disadvantages. For example, the density of the spikes formed in air is lower than that in water, however their conical shape may have better absorption performance than the pillar-shaped spikes formed in water. Therefore, the samples are irradiated in both air and water, in order to compare the optical absorption for different surface geometries.

EXPERIMENTAL SETUP

Amorphous silicon films were deposited on 0.525mm-thick Corning 1747 glass substrates using plasma enhanced chemical vapor deposition (PECVD). The a-Si:H film was deposited at a rate of 60 Å/s in an hydrogen diluted silane environment at 380°C with a hydrogen atomic concentration of around 20 at %.

Femtosecond laser texturing was carried out using a commercial Ti:sapphire oscillator and regenerative amplifier system. The system delivered 130-fs pulses of linearly polarized light at a 1 kHz repetition rate, and a central wavelength of 800 nm. The samples were cleaned with acetone in an ultrasonic cleaner for 5 minutes and then rinsed with methanol and distilled water prior to processing.

The sample was mounted on a three-axis translation stage and irradiated by laser pulses focused by a 60 mm focal-length lens. When changing the environment to water, the sample was placed in a plastic container, the laser beam was focused by the same lens and traveled through 5 mm of distilled water before striking the surface, and the focal plane was positioned below the sample surface in order to obtain the desired spot size of 150µm. For both air and underwater cases, the laser beam was acting normally to the sample surface and the beam spot on the sample surface was circular. To study the morphology, samples were held stationary and irradiated at various fluences (0.2J/cm² to 0.45J/cm²) in air and at higher fluences (1J/cm² to 1.8J/cm²) in water with different numbers of pulses (2-100). In order to measure the absorption and crystallinity, 10×15 mm² areas were processed at specific scanning speeds. The scanning speed, v , is set by the Full width at half maximum (FWHM) of the Gaussian beam profile, d , the number of pulses, N , and the repetition rate of the laser, f , through the relation $v=df/N$ [24].

The untreated and treated samples were observed through SEM. Surface roughness and the distribution of spikes in the treated samples were also examined using an AFM. The optical transmittance and reflectance of the as received a-Si:H films were measured by a spectrophotometer over a wavelength range of 250nm-2500nm which corresponds to the main spectral range of solar irradiation [25]. The reflectance (R in %) and transmittance (T in %) are then used to calculate the absorbance (A in %) of the film: $A=100-R-T$. X-ray diffraction (Cu K_α-line) was used for crystallinity estimation. X-ray photoelectron spectroscopy is used for composition analysis.

RESULTS AND DISCUSSION

The characterization of the as-received a-Si:H thin films is measured in Wang, et al. [8]. The thickness is determined by an ellipsometer to be 1578.6±2.28 nm with a surface roughness of 2.62±0.28 nm where the variation represents standard deviation. The initial surface of the a-Si:H film

appears smooth from SEM image, and the surface average roughness measured by AFM is 2.08 nm, which is close to that measured by the ellipsometer. Therefore, the surface of the as-received a-Si:H film is relatively flat with very little initial texture.

Study of morphology in air

The texture formation mechanism on a-Si:H has been suggested to be quite similar to that for crystalline silicon, since both of them occur under the ablation regime. However, in order not to damage the entire film, thin film samples have a much narrower window of suitable texturing fluences and number of pulses than bulk materials. Also, for the creation of tandem cells for enhanced stability while maintaining the absorption characteristics of amorphous silicon, crystallization of the entire film must be avoided. Therefore, understand the texturing process of a-Si:H thin films is essential for enabling their widespread use in solar cell applications. The formation mechanism of spikes irradiated in water was discussed in previous work by the current authors [8]. In this paper, the mechanism of spike formation in air is discussed.

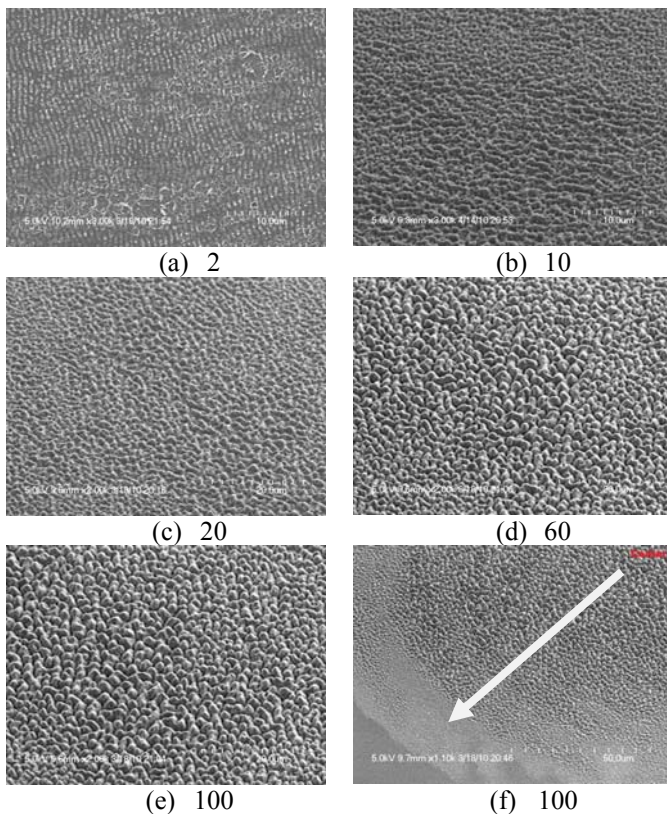


Figure 1. SEM images of a-Si:H film surface after the following number of pulses in air at $0.4\text{J}/\text{cm}^2$ (a)2, (b) 10, (c)20, (d) 60, (e)100, (f) 100, whole view of $1/4$ irradiation area, the arrow in (f) showing the spikes are becoming smaller and denser moving from center to the edge

In order to texture the films without removing them entirely, the amorphous samples are irradiated at stationary locations with fluences from $0.2\text{J}/\text{cm}^2$ to $0.45\text{J}/\text{cm}^2$ and numbers of pulses from 2 to 100. A typical result achieved using a fluence of $0.4\text{J}/\text{cm}^2$ is shown in Fig. 1. The circular surface defects after 2 pulses observed in Fig. 1 (a) are suggested to be generated from burst bubbles that are frozen in place on resolidification of the molten silicon. These bubbles are attributed to a local increase in vaporization of the silicon melt due to defects or impurities at the surface [19]. The periodic ripples are suggested to be formed by the interference between the incident beam and light scattered by those surface defects, which creates capillary waves with periodicity close to the laser wavelength [26]. Figure 1 (b) shows how the periodic ripples disappear after 10 pulses, and instead, perpendicular ridges are formed. The transition could be caused by a surface instability, since the periodic ripples will become long, liquid half-cylinders on the surface after melting; this geometry is not stable if the length of the cylinder is larger than the radius, therefore, the liquid cylinder will be broken into equal-size sections through a process known as cylinder collapse [19]. After 20 pulses, bead-like ripples are formed as shown in Fig. 1 (c), which could be caused by surface tension effects. The above steps are part of the first stage of texture formation. The following stage is the formation of the conical spikes. Figure 1 (d) and (e) show how the conical spikes become sharper and deeper with increasing number of pulses. This is due to the beads formed on the surface concentrating the laser beam into the valleys between them, causing the material around the tips to be preferentially removed and sharp conical spikes to be formed. The result shows that the conical spikes are more regular than those obtained by Nayak, et al. [12]. Figure 1 (f) presents the distribution of the spikes in one quarter of the irradiated area. It can be seen that the spikes are wider, taller and more widely spaced at the center of the laser spot, while they are narrower, shorter, and more closely packed toward the exterior. At the boundary, wavelength-dependent periodic ripples are formed instead of spikes. This may be due to a difference in surface tension at different locations, which depends on many factors, such as melt depth, cooling rate, temperature and pressure, the Gaussian spatial distribution of the laser light.

In order to quantify the characteristics of the features AFM measurements are performed. The average spike height and average spike spacing are determined by measuring each spike height, h , and the average distance, d , to the four closest neighboring spikes. The average spike height and spacing are measured from within an area of $50 \times 50 \mu\text{m}^2$. Figure 2 shows the average spike height correlated with the average spike spacing. The solid line is a curve fit to the data, yielding a linear relation between the two parameters. When the spacing drops to below $1 \mu\text{m}$, the surface is corrugated with no spikes. Figure 3 shows the average spike spacing within the $50 \times 50 \mu\text{m}^2$ area as a

function of fluence when irradiated by 100 pulses. It indicates that higher fluences will lead to an almost linear increase in average spike spacing; therefore, both average spike spacing and height are linearly proportional to the laser fluence, which is different from the nonlinear correlations found for crystalline bulk silicon [27]. When the fluence reaches the ablation threshold ($\sim 0.2\text{J}/\text{cm}^2$) [28], the average spike spacing is close to the laser wavelength. When the fluence is less than the ablation threshold, only periodic ripples are formed on the surface. As the fluence goes higher than $0.2\text{J}/\text{cm}^2$, the average spike spacing becomes larger and larger until it reaches about $2\mu\text{m}$; the center of irradiated area is completely removed if the fluence is more than $0.45\text{J}/\text{cm}^2$ (not shown).

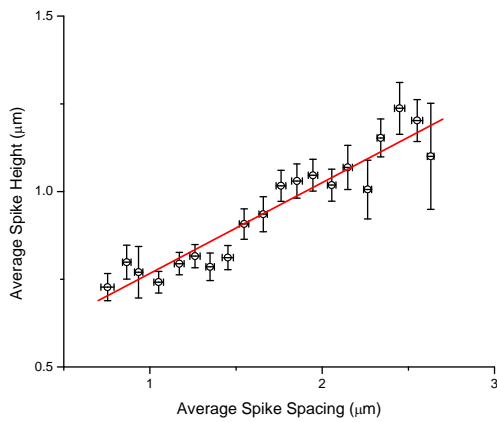


Figure 2. Dependence of average spike height on average spike spacing after laser treated in air, determined from an area of $50 \times 50 \mu\text{m}^2$ at the processing center ($0.4\text{J}/\text{cm}^2$, 100 pulses). The solid straight line is a linear fitting to the measurement, error bars indicate standard deviation

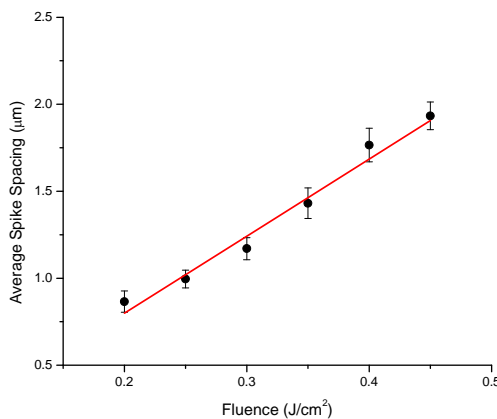


Figure 3. Dependence of average spike spacing on laser fluence for a fixed number of pulses (100 pulses) after treated in air, determined from an area of $50 \times 50 \mu\text{m}^2$ at the processing center, error bars indicate standard deviation

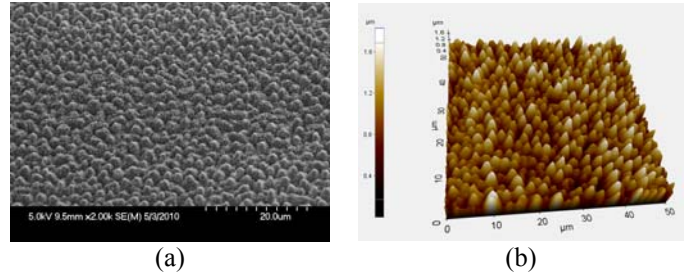


Figure 4. (a) SEM image and (b) AFM image of surface of a-Si:H film laser irradiated in air, ($0.4\text{J}/\text{cm}^2$, $1\text{mm}/\text{s}$), showing texturing with conical spikes on the surface

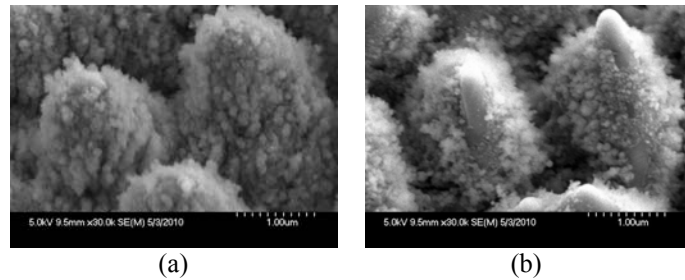


Figure 5. Comparison of textured spikes made by (a) scanning ($0.4\text{J}/\text{cm}^2$, $1\text{mm}/\text{s}$) and (b) stationary ($0.4\text{J}/\text{cm}^2$, 100 pulses) pulsing, showing nanoparticles distributed on the whole spike after laser scanning in air

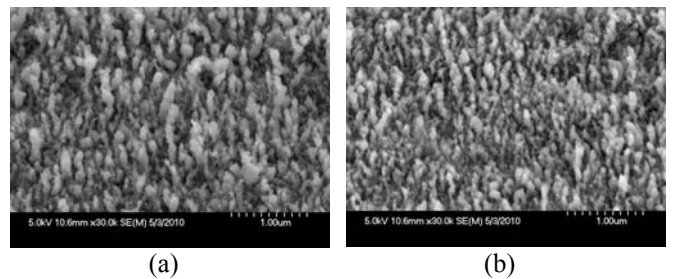


Figure 6. Comparison of textured spikes made by (a) scanning ($1.2\text{J}/\text{cm}^2$, $2\text{mm}/\text{s}$) and (b) stationary ($1.2\text{J}/\text{cm}^2$, 50 pulses) pulsing, showing similar pillar-shaped spikes textured on the both sample surfaces

Surface morphology after laser scanning

When observed optically, the surface of the processed a-Si:H film is much darker than the original shiny reddish gray color which shows that the textured surface has the capability to trap light which greatly reduces the visible light reflection. Figure 4 (a) shows the SEM images of the surface processed at a fluence of $0.4\text{J}/\text{cm}^2$ and a speed of $1\text{mm}/\text{s}$ in air, and the spikes look similar to those formed during stationary spot irradiation (Fig. 1). The AFM measurement in Fig.4 (b) shows that conical spikes are formed on the sample surface with an average height of $0.922 \pm 0.0487\mu\text{m}$ and an average spike spacing of $1.886 \pm 0.0824\mu\text{m}$ where the variation represents standard deviation. Figure 5 (a) and (b) show high magnification

SEM images of scanned and stationary processed sample surfaces; there are two visible differences between these two samples. First, the spikes on the stationary sample have a smooth conical shape at the tips while those on the scanned sample look blunter and lack this smooth conical shape. Second, the scanned sample has a larger amount of nanoscale particles spread across the spike surfaces. The nanoscale particles on the scanned sample are made of redeposited material from the ejected plasma plume and can potentially lead to light scattering. On a stationary sample, most of this debris lies away from the area where the surface morphology forms, and deposits as a ring around the irradiation spot [29]. The presence of the conical tips on the stationary processed a-Si:H surface could be caused by resolidified droplets of redeposited molten silicon. The droplets at the tips are flowing around the spike surface towards the bottom due to gravity and a conical tip is formed after resolidification.

Typical conditions for a sample treated in water are chosen to be a fluence of 1.2J/cm² and 50 pulses, since the sample surface geometries are similar under the laser processing conditions from 1J/cm² to 1.8J/cm² in water, which will lead to similar absorptance spectra [8]. Figure 6 shows the SEM images of both a scanned sample surface treated at a fluence of 1.2 J/cm² at 2mm/s and a stationary sample treated at 1.2J/cm² at 50 pulses in water and similar spike formations are observed. The reason is that water convection and the motion of decomposed bubbles contribute to the reduction of debris redeposition. Therefore, the spike surfaces in both samples are smooth. The average spike height and spacing of scanned sample measured by AFM are 391.75±2.612 nm and 218.63±3.867 nm, respectively, which are close to those measured on stationary samples [8]; the variation represents standard error.

Effect of laser processing on absorption

Figure 7 shows the comparison of absorptance measurements of untreated and treated samples with surface texture consisting of low-density conical spikes formed in air and high-density pillar-shaped spikes formed in water. A dramatic increase in the absorptance can be seen for the treated a-Si:H films over the entire spectrum. The absorptance spectra for both treated samples go up to more than 90% from UV wavelengths to the band gap of a-Si:H (730nm) due to multiple reflections enabled by the surface texture, and decrease to around 45% and 30% in the below-band-gap region, for the air and water treated samples respectively. In the above-band-gap range, the absorption for the samples processed under different conditions as a function of wavelength show different trends. The increase in absorptance for the untreated sample from UV wavelengths to the band gap is mainly caused by the material's optical properties, which indicates that the absorption coefficient increases with increasing

wavelength. However, the opposite trend is observed in the sample treated in air which may be caused by light scattering by the nanoparticles attached to the surface of the conical spikes (Fig. 5). According to Rayleigh scattering theory, when the radius of the particle is much smaller than the wavelength of the incident light, the intensity of scattered light is inversely proportional to the fourth power of the wavelength [30]

$$I(\lambda)_{scattering} \propto \frac{I(\lambda)_{incident}}{\lambda^4} \quad (3)$$

where I and λ are intensity and wavelength, respectively.

Therefore, at shorter wavelengths, a larger fraction of the incident light is scattered by the nanoparticles, which causes the highest absorptance to occur at the shortest wavelength. The absorptance spectrum of the sample treated in water is almost flat, which can be caused by much fewer nanoparticles being generated on the spikes due to the influence of water, thus a smaller fraction of light is scattered.

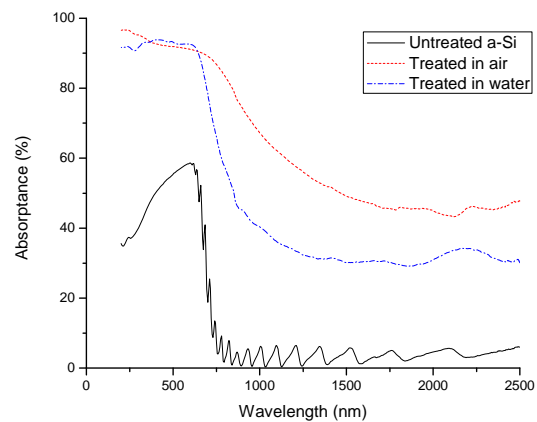


Figure 7. Comparison of absorptance spectra of as-received and laser treated a-Si:H films at fluences of 0.4J/cm² (scan speed 1mm/s) and 1.2J/cm² (scan speed 2mm/s) in air and water by spectrophotometry, showing increase in absorptance over entire spectrum for both treated samples

For untreated a-Si:H, light at wavelengths longer than 730nm does not contain enough energy to promote an electron from the valence band to the conduction band which results in the absorptance being close to zero. The differences in the below-band gap absorptance of the treated a-Si:H samples could be attributed to different levels of crystallinity (band gap of nc-Si:H is 1.1eV or 1100nm) [8] which broadens the absorption range to 1100nm while the textured surface introduces light trapping through multiple reflections as well as scattering by the nanoparticles. Moreover, the water environment may introduce less impurities and defects during laser processing which can cause fewer sub-band gaps to form, which causes the material to absorb a smaller fraction of

light with longer wavelengths compared to the sample treated in air. The reason why the absorbance starts decreasing at 730nm rather than staying constant to 1100nm is due to the material remaining primarily amorphous with a band-gap of 730nm [8]. In the below-band gap range, unlike for untreated a-Si:H, the absorbance curves for the treated films do not oscillate. The multiple reflections caused by the textured surface change the transmitted light paths through the film such that rays will not be reflected back along their original paths, eliminating internal interference. From the discussion above, it is shown that the absorption can depend on the surface geometry, such as spike shape, density and attached nano-particles, as well as crystallinity and impurity concentrations.

Effect of laser processing on crystallinity

In order to study the crystallization of the treated films, x-ray diffraction patterns were taken for the untreated and treated a-Si:H films in air and water and are shown in Fig. 8. The spectra have been shifted vertically for clarity. All the spectra show an amorphous peak around $2\theta=25^\circ$, which is caused by the internal constructive interference of the amorphous Si network. Three peaks at around $2\theta=29^\circ$, 47° and 56° emerge after processing in air which indicate a structural change after laser irradiation and can be indexed to the (111), (220) and (311) crystalline orientations of silicon. During femtosecond laser processing an ultrafast non-thermal disorder-to-disorder phase transition occurs within a few picoseconds of the laser pulse which cannot lead to crystallization [8]. The material is then partially melted due to thermal diffusion after energy transfer from the excited electrons to the material. The resolidification of the melted layer proceeds via vertical growth from the remaining un-melted material and results in random crystal orientations due to the amorphous structure of the film. According to the silicon powder diffraction file, the highest three intensities of x-ray diffraction are for the (111), (220) and (311) orientations and are the same as observed in Fig. 11. The crystallization is considered to be under the partial melting regime, resulting in no preferential orientation during solidification. This suggests that the laser irradiated film becomes a mixture of $\mu\text{-Si:H}$ and a-Si:H with most of the $\mu\text{-Si:H}$ believed to be contained within the top melted surface. However, the XRD pattern also shows that the sample treated in water at 1.2J/cm^2 with a scan speed of 2mm/s has no crystallinity.

In order to further understand the effect of laser processing parameters, fluence and scan speed, on crystallinity in water, a film was treated with a lower fluence (0.5J/cm^2) at 2mm/s and at a higher scanning speed (25mm/s). The XRD patterns are shown in Fig. 9. Only the sample treated at 0.5J/cm^2 with scan speed of 25mm/s has two small peaks that can be indexed to the (111) and (220) orientations of silicon. The reason is due to the higher cooling rate in a water environment than in air; the melted

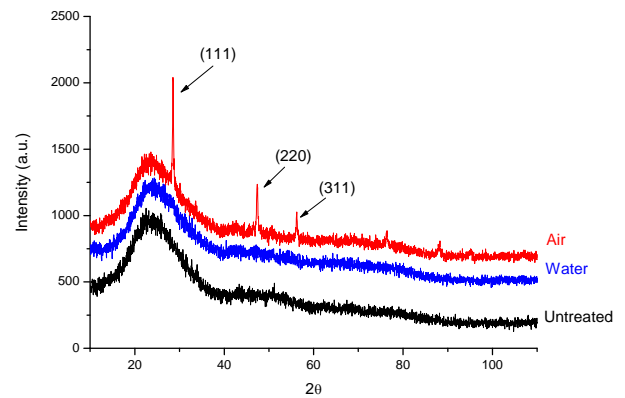


Figure 8. X-ray diffraction spectra of as-received a-Si:H film, laser treated films at fluences of 0.4J/cm^2 and 1.2J/cm^2 in air and water, respectively. All the spectra show an “amorphous peak” at around $2\theta=25^\circ$ and no signs of crystallinity for the untreated sample and that treated in water. Sample treated in air shows three different peaks for (111), (220) and (311) orientation of silicon. The spectra have been shifted for clarity

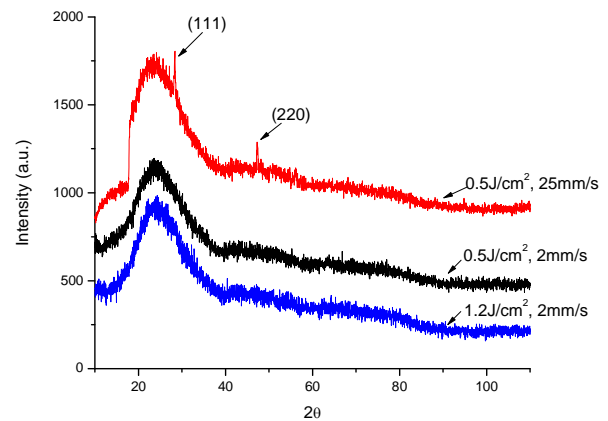


Figure 9. X-ray diffraction spectra of a-Si:H films laser treated at fluences of 0.5J/cm^2 and 1.2J/cm^2 , and scan speeds of 2mm/s and 25mm/s in water. An “amorphous peak” around $2\theta=25^\circ$ is observed for all samples. Sample processed at 0.5J/cm^2 and 25mm/s shows existence of two peaks for (111) and (220) orientation of silicon, showing the effect of different laser parameters on crystallinity

silicon resolidifies so quickly that much less material is able to crystallize. The sample processed at the same fluence, 0.5J/cm^2 , but lower scan speed of 2mm/s has no crystallinity; the reason could be the higher pulse overlap during processing. Daminelli, et al. [18] showed that the ablation threshold of silicon decreases with increasing number of pulses due to modification of the absorption behavior of the film such that subsequent surface texturing occurs at fluence levels lower than for previous pulses.

Processing with this decreased threshold caused by higher overlap can be considered to be equivalent to processing at a higher fluence and lower overlap. Figure 10 shows the XRD pattern of samples treated at the same scan speed, 25mm/s, but different fluences from 0.5 to 0.8J/cm². It can be seen that the crystallinity decreases with increasing fluence, and fluences larger than 0.7J/cm² do not introduce crystallinity. The thermal effects of laser processing can be described using a model that is based on one-dimensional heat flow given by [31],

$$c_s(T)\rho_s(T)\frac{\partial T(x,t)}{\partial t} = \frac{\partial}{\partial x}\left[\kappa(T)\frac{\partial T(x,t)}{\partial x}\right] + S(x,t) \quad (4)$$

where $T(x,t)$ is the temperature distribution, $c_s(T)$ is the specific heat, $\rho_s(T)$ is the density, $\kappa(T)$ is the thermal conductivity and $S(x,t)$ is the source which is proportional to the energy absorbed by the surface layer estimated by,

$$S(x,t) = \alpha(t)I(x,t), \quad I(x,t) = I_0(t)[1 - R(T)]e^{-\alpha(T)x} \quad (5)$$

where $R(T)$ is the reflectivity, $\alpha(t)$ is absorption coefficient and $I_0(t)$ is the laser pulse intensity.

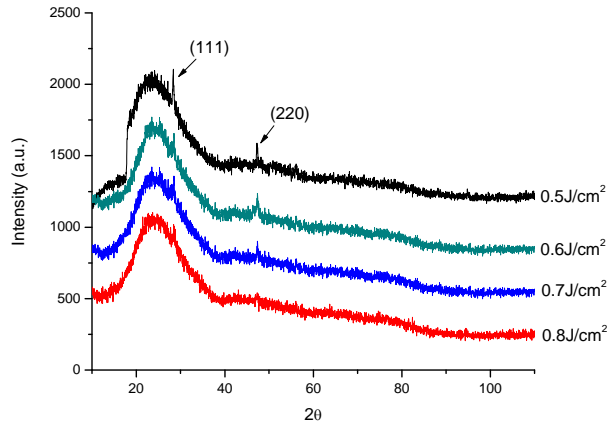


Figure 10. X-ray diffraction spectrum of laser treated a-Si:H film at different fluences from 0.5J/cm² to 0.8J/cm² with the same scan speed of 25 mm/s in water. An “amorphous peak” around 2θ=25° is observed for all samples. Existence of two overall different peaks for (111) and (220) orientation of silicon, showing that the crystallinity decreases with increasing of fluence

As discussed in [8], thermal melting occurs underneath the ablated layer and is caused by thermal diffusion, thus the higher the fluence, the thicker the ablated layer, and the deeper the thermally melted layer will be. Based on Eq. (4), the influence of laser fluence on the temperature distribution along the depth of the film is shown in [31]; it can be seen that the temperature gradient increases with increasing fluence and depth into the film. Thus the thermal melting caused by higher fluences will introduce steeper temperature gradients compared to the lower fluence treated

samples and can be solidified quicker. Therefore, the higher fluence can cause a higher cooling rate, which accelerates the cooling/resolidification process and reduces crystallinity.

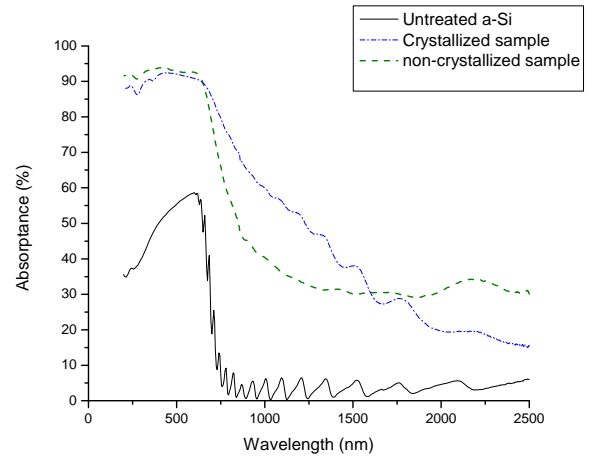


Figure 11. Comparison of absorbance spectra of as-received and laser irradiated a-Si:H films with and without crystallinity at different fluences and scanning speeds (0.5J/cm² at 25mm/s, 1.2J/cm² at 2mm/s) in water, showing the effect of crystallinity on absorption

Effect of different factors on absorption

The average spike height and spacing of the sample treated at a fluence of 0.5J/cm² with a scan speed of 25mm/s in water are determined by AFM to be 138±2.58 nm and 216±6.77 nm, respectively, where the variation represents standard error. From SEM images [8], the surface texture is visually similar to the samples treated at a higher fluence of 1.2J/cm² at a scan speed of 2mm/s (Fig. 6), moreover, the spike spacing measured through AFM of the two samples are also close, and spike heights are 138nm and 391nm, respectively. Therefore, the absorbance of these two samples should be similar if both are not crystallized, since the spike height does not affect the absorption as discussed above. In fact, however, the sample processed at 25mm/s is partially crystalline while the sample processed at 2mm/s is not. The comparison of these two samples can show the effect of crystallization on absorption. Figure 11 shows the absorbance versus wavelength for both the crystallized and non-crystallized samples, and the untreated sample is also included for comparison. As seen, due to the similar surface texture, in the above-band-gap region the absorbance spectra of both laser treated samples are almost the same, no matter how deep the spikes are. The change in crystallinity is not significant here since the majority of the material is still a-Si:H after processing. The highest absorbance from the band gap to around 1600nm is for the crystallized sample processed at 0.5J/cm², followed by the non-crystallized sample treated at 1.2J/cm²; the reason could be that the

crystallized portion of the sample has a band gap of 1.1 eV, which helps to absorb light with wavelengths up to 1100nm. Moreover, the crystallized sample has a thicker a-Si:H layer due to the formation of shorter spikes and the resulting higher defect and impurity concentration could also cause higher absorption. The reason that the crystallized sample has lower absorption for wavelengths above 1600nm is not well understood at this point. However, based on the solar radiation spectrum, the radiation intensity in this range is a very small portion of the total intensity [25], which suggests that lower absorption at these higher wavelengths will only have a small effect on the total energy absorption. Therefore, over the entire range of the spectrum, it can be concluded that with similar surface texture, a crystallized sample will have better absorption performance due to the combination of both surface texturing and crystallization.

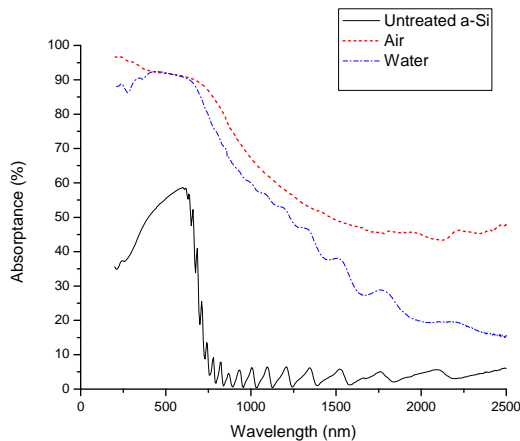


Figure 12. Comparison of absorbance spectra of as-received and laser irradiated a-Si:H film in air ($0.4\text{J}/\text{cm}^2$, $1\text{mm}/\text{s}$) and water ($0.5\text{J}/\text{cm}^2$, $25\text{mm}/\text{s}$), showing the effect of different factors, such as surface geometry, crystallinity and processing medium on absorption

In order to compare the effect of other factors, such as surface geometry and crystallinity, absorbance spectra for samples treated in air at a fluence of $0.4\text{J}/\text{cm}^2$ and a scan speed of $1\text{mm}/\text{s}$ and in water at a fluence of $0.5\text{J}/\text{cm}^2$ with a scan speed of $25\text{mm}/\text{s}$ are shown in Fig. 12. It is observed that the sample treated in air has better absorbance performance over the entire spectrum. In the above-band-gap region, the conical spikes and attached nano-particles formed on the sample treated in air can induce greater light reflection and scattering between the spikes, which play a more important role in absorbance than spike density, which is higher for the water treated sample. The conical spikes, greater crystallinity, as well as the defects and impurities formed during the laser processing in air introduce greater numbers of reflections, a wider absorption spectrum, and sub-band gaps. These effects all work to

increase the absorbance in the below-band-gap region to above that achieved by the sample treated in water. Therefore, with a sufficient thickness of a-Si:H left after laser processing for absorption, a treated sample surface having regular spike shapes with sharper angles, attached nano-particles, more crystallinity, greater defect and impurity concentrations, and larger spike densities will have better absorbance.

Compared to the absorbance spectra of the crystalline silicon wafers laser treated in different background gas environments as show by Younkin, et al. [15], it can be seen that both textured crystalline bulk silicon and a-Si:H thin films in air have similar absorbance performance in the above-band-gap region. In the below-band-gap range, the absorbance of crystalline silicon drops quickly to almost zero, but for the a-Si:H film, the absorbance only drops to around 45% and remains more or less constant with increasing wavelength. Therefore, comparing the thicknesses of a few hundred microns for crystalline silicon and $1.6\mu\text{m}$ for a-Si:H, it can be concluded that a-Si:H thin films have greater absorbance while being more economical than crystalline bulk silicon and may be ideal for solar cell fabrication.

CONCLUSION

In conclusion, it has been demonstrated that simultaneously improving the absorbance of sunlight and the stability against the SWE of a-Si:H thin films is possible through femtosecond laser irradiation in both air and water. Absorbance enhancement is caused by light trapping based on the surface geometry changes, as well as increased defect and impurity concentrations caused by laser processing. The change in crystallinity after processing reduces the thickness of the a-Si:H layer but may allow for greater stability in a-Si:H-based solar cells and broadens the absorbance range to 1100nm. Furthermore, the correlation between the crystallinity and scan speed and fluence when treated in water have been investigated; the crystallinity decreases with increasing laser fluence and decreasing scan speed, which may be due to the increased cooling rate caused by the higher surface temperature and temperature gradient. Finally, the absorbance spectra indicate that the samples treated in air with regular conical spikes, crystallization and high defect and impurity concentration have the best absorption performance over the solar radiation spectrum. Compared with the absorbance of laser textured crystalline bulk silicon, it can be concluded that femtosecond laser processing of a-Si:H thin films may allow for more efficient and economical solar cell applications.

ACKNOWLEDGMENT

The use of material characterization equipment at the Center for Functional Nanomaterials, Brookhaven National

Laboratory and at Materials Research Science and Engineering Center, Columbia University is gratefully acknowledged.

REFERENCES

- [1] Luque A, Hegedus S (2003) *Handbook of Photovoltaic Science and Engineering*. Wiley, UK, Chap. 7-8.
- [2] Chopra KL, Paulson PD, Dutta V (2004) Thin-film solar cells: an overview. *Prog. Photovolt: Res. Appl.* 12, 69-92.
- [3] Kazmerski LL (2006) Solar photovoltaics R&D at the tipping point: A 2005 technology overview. *Journal of Electron Spectroscopy and related Phenomena* 150, 105-135.
- [4] Miles RW, Hynes KM, Forbes I (2005) Photovoltaic solar cells: An overview of state-of-the-art cell development and environmental issues. *Progress in Crystal Growth and Characterization of Materials* 51, 1-42.
- [5] Staebler DL, Wronski CR (1980) Optically induced conductivity changes in discharge-produced hydrogenated amorphous silicon. *Journals of Appl. Physics* 51(6).
- [6] Martirosyan KhS, Hovhannisyanyan AS, Arouiounian VM (2007) Calculation of reflectance of porous silicon double-layer antireflection coating for silicon solar cells. *Physica Status Solid (c)* 4(6), 2103-2106.
- [7] Hylton JD, Burgers AR, Sinke WC (2004) Alkaline etching for reflectance reduction in multicrystalline silicon solar cells. *Journal of the Electrochemical Society* 151(6), G408-G427.
- [8] Wang H, Kongsuwan P, Satoh G, Yao YL (2010) Femtosecond laser-induced surface texturing and crystallization of a-Si:H thin film. *Proceedings of the 2010 International Manufacturing Science and Engineering Conference, Erie, PA*, MSEC2010-34271.
- [9] Crouch CH, Carey JE, Warrender JM, Aziz MJ, Mazur E, Genin FY (2004) Comparison of structure and properties of femtosecond and nanosecond laser-structured silicon. *Applied Physics Letters* 84(11), 1850-1852.
- [10] Kolodziej A (2004) Staebler-Wronski effect in amorphous silicon and its alloys. *Opto-electronics review* 12(1), 21-32.
- [11] Yamamoto K, et al., (2004) A high efficiency thin film silicon solar cell and module. *Solar Energy* 77, 939-949.
- [12] Nayak BK, Gupta MC (2007) Femtosecond-laser-induced-crystallization and simultaneous formation of light trapping microstructures in thin a-Si:H films. *Appl. Phys. A* 89, 663-666.
- [13] Zheng HY, Jiang ZW (2010) Femtosecond laser micromachining of silicon with an external electric field. *J. of Micromechanics and Microengineering* 20, 017001.
- [14] Jiang L, Tsai HL (2003) Femtosecond laser ablation: challenges and opportunities. *Proceeding of NSF Workshop on Research Needs in Thermal, Aspects of Material Removal, Stillwater, OK*, 163-177.
- [15] Younkin R, Carey JE, Mazur E, Levinson JA, Friend CM (2003) Infrared absorption by conical silicon microstructures made in a variety of background gases using femtosecond-laser pulses. *J. of Applied Physics* 93(5), 2626-2629.
- [16] Sheehy MA, Winston L, Carey JE, Friend CM, Mazur E (2005) Role of the background gas in the morphology and optical properties of laser-microstructured silicon. *Chem. Mater* 17, 3582-3586.
- [17] Shen MY, Crouch CH, Carey JE, Mazur E (2004) Femtosecond laser-induced formation of submicrometer spikes on silicon in water. *Applied Physics Letters* 85(23), 5694-5696.
- [18] Daminelli G, Kruger J, Kautek W (2004) Femtosecond laser interaction with silicon under water confinement. *Thin Solid Films* 467, 334-341.
- [19] Tull BR, Carey JE, Mazur E, McDonald JP, Yalisove SM (2006) Silicon surface morphologies after femtosecond laser irradiation. *MRS Bulletin* 31(8), 626-633.
- [20] Tan B, Venkatakrishnan K (2006) A femtosecond laser-induced periodical surface structure on crystalline silicon. *J. of Micromech. and Microeng.* 16, 1080-1085.
- [21] Yagi T, Uraoka Y, Fuyuki T (2006) Ray-trace simulation of light trapping in silicon solar cell with texture structures. *Solar Energy Mat. & Solar Cells* 90, 2647-2656.
- [22] Halbwax M, Sarnet T, Delaporte P, Sentis M, Etienne H, Torregrosa F, Vervisch V, Perichaud I, Martinuzzi S (2008) Micro and nano-structure of silicon by femtosecond laser: application to silicon photovoltaic cells fabrication. *Thin Solid Films* 516, 6791-6795.
- [23] Hua X, Zhang Y, Wang H (2010) The effect of texture unit shape on silicon surface on the absorption properties. *Solar Energy Materials & Solar Cells* 94, 258-262.
- [24] Crouch CH, Carey JE, Mazur E, Fenin FY (2004) Infrared absorption by sulfur-doped silicon formed by femtosecond laser irradiation. *Appl. Phys. A* 79, 1635-1641.
- [25] Goetzberger A, Knobloch J, Voss B (1998) *Crystalline Silicon Solar Cells*. Wiley, Chichester, Chap. 2.
- [26] Sipe JE, Young JF, Preston JS, Van Driel HM (1983) Laser-induced periodic surface structure. I. theory. *Physical Review B* 27(2), 1141-1154.
- [27] Her TH, Finlay RJ, Wu C, Mazur E (2000) Femtosecond laser-induced formation of spikes on silicon. *Applied Physics A* 70, 383-385.
- [28] Kruger J, Kautek W (1995) Femtosecond-pulse laser processing of metallic and semiconducting thin films. *SPIE* 2403, 436-447.
- [29] Carey JE (2004) *Femtosecond-laser Microstructuring of Silicon for Novel Optoelectronic Devices*. Ph.D dissertation, Harvard University.
- [30] Steen W (2003) *Laser Material Processing*, 3rd edition, Springer-Verlag, London, 76-77.
- [31] Palani IA, Vasa NJ, Singaperumal M (2008) Crystallization and ablation in annealing of amorphous-Si thin film on glass and crystalline-Si substrates irradiated by third harmonics of Nd³⁺: YAG laser. *Material Science in Semiconductor Processing* 11, 107-116.